CORROSION SIMULATION FOR THE PROCESS INDUSTRY

N. Sridhar
CNWRA, Southwest Research Institute
6220 Culebra Road
San Antonio, Texas

A. Anderko
OLI Systems, Inc.
One American Parkway
Morris Plains, NJ

ABSTRACT

The paper describes several approaches to perform computer simulation of corrosion occurring in the chemical process industries. While the present state of the art does not permit simulating all modes of corrosion observed in process systems, useful insights can be gained at the design stage by the inclusion of corrosion simulation tools. A thermodynamic speciation model coupled to electrochemical kinetic model is used to calculate the uniform corrosion rates in a variety of mixed acid systems. Such a model can also compute the corrosion potential; an important parameter that can determine the occurrence of a variety of localized corrosion processes. For systems undergoing localized corrosion, a semi-empirical model, involving repassivation and corrosion potentials is described. Other approaches to corrosion prediction are described briefly. Areas for further development are identified.

Keywords: Corrosion, acids, process simulation, thermodynamics, corrosion potential, repassivation potential, stainless steel, nickel-base alloys, chemical process industry

INTRODUCTION

In charting the evolution of the process industry over the next 20 or so years Keller and Bryan[1] delineate seven themes for future process improvements:
- Raw material cost reduction

- Capital investment reduction
- Energy use reduction
- Increased process flexibility and inventory reduction
- Process safety
- Increased attention to quality
- Better environmental performance

They argued that three quarters of the products that will be sold in the year 2020 will be produced with equipment operating in 1999 and that much of the process engineering improvements will also be done using the existing units. This is because capital costs constitute 25-50 percent of the total product sales price. In its *Technology Roadmap*,[2] The Materials Technology Institute of the Chemical Process Industries, Inc. identified the prediction of material performance in complex chemical systems without empirical tests as a priority research need and a key barrier to process improvement. This assessment, combined with the seven themes outlined by Kellar and Bryan, would suggest that the process engineers in the future will have to contend with the need to use the same equipment to implement new processes or manufacture new products while ensuring safe and trouble-free operation. Additionally, the time period between process conception and commercialization has become shortened, so that the process engineers do not always have the luxury of the traditional scale-up route involving laboratory development and pilot plant testing[3].

Generally, materials selection for new processes is made through a combination of previous process experience, laboratory testing, or plant testing in a related process or pilot plant. Staehle[4] has delineated the following steps in a corrosion based design approach:

- Environment definition
- Material definition (characterization)
- Failure mode assessment
- Failure criteria
- Statistical treatment and scale-up
- Accelerated testing
- Prediction of performance
- Monitoring and feedback

This paper discusses approaches to defining the environment causing the corrosion and assessing the failure modes. Ideally, corrosion based design approach should be a part of process simulation software because these simulation tools are often used by chemical engineers in designing new processes. However, the process simulation software available today does not incorporate models to evaluate the performance of process equipment[3], which would make risk assessment and informed investment decisions possible. A variety of heuristic methods (expert systems, neural network models) have been published to tackle this problem, but none are completely satisfactory for new applications.

The objective of the paper is to review the process corrosion simulation tools that are available and describe the applications and limitations of each of these tools. The need for incorporating corrosion modeling in process simulation tools to integrate corrosion in design and to conduct risk based inspection will be mentioned. Some historical aspects of process corrosion modeling will be described. The simulation approaches that will be reviewed in this paper will include mechanistic models (including thermodynamic and kinetic models), empirical models, and heuristic approaches. The limitations and advantages of these approaches will be summarized.

MECHANISTIC AND SEMI-EMPIRICAL MODELS

Thermodynamic Simulation of Processes

Thermodynamic modeling of aqueous streams forms the basis for both process and corrosion simulation. In process simulation, emphasis is put on performing material and heat balances for processes composed of various unit operations in order to design or optimize the processes of interest. In corrosion simulation, the focus is on understanding and predicting the effect of process conditions on the behavior of engineering metals that are in contact with aqueous streams. Thermodynamic models make it possible to predict the behavior of systems including:

(1) The presence, amounts and compositions of various phases in the system (i.e., aqueous, vapor, nonaqueous liquid, multiple solids);
(2) Detailed speciation in the aqueous phase, which is necessary to predict the concentrations and activities of corrosive species (e.g., H^+ or CI^- ions, oxygen molecules, etc.);
(3) The response of the system to changes in external conditions such as temperature, pressure or overall composition; this may also include the change in the behavior of the system that may result from the dissolution of corroding metals.

Thermodynamic modeling of electrolyte solutions has been an active area of research for several decades. It is beyond the scope of this work to review all approaches that have been published in the literature. Instead, the reader is referred to the reviews of Pitzer[5] and Loehe and Donohue[6]. Here, we will briefly review the fundamental concepts of thermodynamic modeling. Then, we outline a speciation-based model, which is appropriate for reproducing both chemical and phase equilibria in aqueous systems[7,8].

For realistic simulation of aqueous systems, it is of utmost importance to consider all species that may form in the system. Such species include solvent molecules, simple ions, ion pairs, complex ions, solid species, etc. A comprehensive treatment of such systems has to include both standard-state properties and solution nonideality. The standard-state properties reflect the properties of individual species in the infinite dilution limit whereas the solution nonideality is a manifestation of interactions between species at finite concentrations[7,8]. In a multicomponent system, the partial molal Gibbs energy of the i-th species is related to the molality (m_i) by

$$\overline{G}_i = \overline{G}_i^0 + RT \ln m_i \boldsymbol{g}_i \qquad (1)$$

where $\overline{G}_i^0$ is the standard-state partial Gibbs energy and γ_i is the activity coefficient. Thus, the thermodynamic properties of the system can be calculated if the standard-state Gibbs energies are available for all species as functions of temperature and pressure (i.e., $\overline{G}_i^0(T,P)$) and the activity coefficients are known as functions of the composition vector $\mathbf{m}$ and temperature (i.e., $\gamma_i(\mathbf{m},T)$). From basic thermodynamics, the standard-state Gibbs energy of formation $\overline{G}_i^0(T,P)$ can be calculated as a function of temperature and pressure if the following data are available:

(1) Gibbs energy of formation at a reference temperature and pressure (usually, $T_r = 298.15$ K and $P_r = 1$ bar);
(2) Enthalpy of formation at T_r and P_r;
(3) Entropy at T_r and P_r;
(4) Heat capacity as a function of temperature and pressure and

(5) Volume as a function of temperature and pressure

The key to representing the standard-state properties over substantial temperature and pressure ranges is the accurate knowledge of the heat capacity and volume. For this purpose, the Helgeson-Kirkham-Flowers-Tanger[9,10] equation of state is convenient. This equation accurately represents the standard-state thermodynamic functions for aqueous, ionic or neutral, species as functions of both temperature and pressure. In its revised form[10], the HKFT equation is capable of reproducing the standard-state properties up to 1000 °C and 5 kbar.

The HKFT equation is based on the solvation theory and expresses the standard-state thermodynamic functions as sums of structural and solvation contributions, the latter being dependent on the properties of the solvent (i.e., water). It gives expressions for the standard partial molal volume and heat capacity. Then, the remaining functions are obtained by standard thermodynamic integration using the values of the Gibbs energy, enthalpy and entropy at reference temperature and pressure as integration constants.

If the HKF equation parameters are not available from the regression of experimental data, they can be estimated. For this purpose, Shock and Helgeson[11,12] presented correlations for most solution species except for complexes. Sverjensky[13] developed an estimation method for several classes of complexes. In addition to the HKF equation parameters, these methods make it possible to predict the reference-state enthalpy and entropy if the reference-state Gibbs energy is known. These and other estimation techniques have been reviewed in detail by Rafal et al.[8]

Among numerous activity coefficient models reported in the literature, the modified Bromley[14] (1972) model combines relative simplicity with applicability over wide ranges of concentration. The Bromley equation is a combination of the Debye-Hückel term for long-range electrostatic interactions and a semi-empirical expression for short-range interactions between cations and anions. In a multicomponent system, the activity coefficient of an ion i is given by

$$\log g_i = \frac{-Az_i^2 I^{1/2}}{1+I^{1/2}} + \sum_j^{NO}\left[\frac{|z_i|+|z_j|}{2}\right]^2 \left[\frac{(0.06+0.6B_{ij})|z_i z_j|}{\left(1+\frac{1.5}{|z_i z_j|}I\right)^2} + B_{ij} + C_{ij}I + D_{ij}I^2\right]m_j \qquad (2)$$

where A is the Debye-Hückel coefficient which depends on temperature and solvent properties, z_i is the number of charges on ion i, I is the ionic strength (i.e., $I = 0.5\sum z_i^2 m_i$), NO is the number of ions with charges opposite to that of ion i, and B_{ij}, C_{ij} and D_{ij} are empirical, temperature-dependent cation-anion interaction parameters. Bromley's[14] original formulation contains only one interaction parameter, B_{ij}, which is sufficient for systems with moderate ionic strength. For concentrated systems, the two additional coefficients C_{ij} and D_{ij} usually become necessary. The three-parameter form of the Bromley model[14] is capable of reproducing activity coefficients in solutions with ionic strength up to 30 mol/kg. The temperature dependence of the B_{ij}, C_{ij} and D_{ij} parameters is usually expressed using a simple quadratic function.

The Bromley[14] model is restricted to interactions between cations and anions. For ion-molecule and molecule-molecule interactions, the well-known model of Pitzer[15] (1973) is used. In the absence of sufficient experimental data, reasonable predictions can be made using a method due to Meissner[16], which makes it possible to extrapolate the activity coefficients to higher ionic strengths based on only a single, experimental or predicted, data point.

Application of electrolyte thermodynamics to simulation of industrial processes

There are numerous processes in the chemical process industries in which the behavior of electrolytes plays a major role. Such processes involve

- Flue gas scrubbing systems (e.g., scrubbing of Cl_2 or SO_2)
- Sour water strippers and amine scrubbers, which remove components such as carbon dioxide, hydrogen sulfide, ammonia, etc.
- Treatment of wastewater streams including neutralization, precipitation of heavy metals and other undesirable ions, etc.
- Application of heavy brines as completion fluids in petroleum production
- Treatment of produced brines to remove organic acids and volatile components
- Squeeze processes for oil and gas producing reservoirs
- Manufacture of various inorganic materials by crystallization from solution
- Seawater desalination
- Electrochemical manufacturing processes such as the chlor-alkali process
- Plating processes
- Refrigeration technology, which involves the use of concentrated brines
- Several processes in the pulp and paper industry
- Hydrometallurgical processes, which involve the treatment of ores with aqueous solutions
- Cooling towers

For the simulation of such processes, electrolyte thermodynamic models are coupled with general process flowsheeting tools. For example, the model described above is incorporated into OLI Systems' Environmental Simulation Program (ESP) and can be used in conjunction with general-purpose process simulation tools such as Aspen Plus (Aspen Technology).

General Corrosion Simulation

This section will describe modeling general corrosion using electrochemical kinetic rate laws and thermodynamic speciation. The electrochemical models include a mathematical representation of the partial electrochemical reactions that are responsible for corrosion. In view of the complex nature of corrosion processes, such models are unavoidably complex with respect to their mathematical structure and procedures for evaluating model parameters. However, they offer a chance of making reasonable predictions at conditions that go beyond the range of experimental data that were used to obtain model parameters. General corrosion models of this kind have been developed for CO_2 corrosion of carbon steels[17,18], metals covered with thin layers of water[19], and several systems including heavy brines, CO_2/H_2S systems, aerated industrial water systems with inorganic inhibitors, acid mixtures, etc.[20-22]. In this section, we outline the main features of a general corrosion model that has been developed at OLI Systems[21,22]. Then, we present selected examples that illustrate the capabilities of the model.

Structure of the model. The starting point for corrosion analysis is the computation of speciation in the investigated system. For this purpose, the thermodynamic model outlined above is used. This model is used to predict the concentrations and activities of both ionic and neutral species in

multicomponent systems that may contain an aqueous phase, any number of solid phases and, if necessary, a vapor and a nonaqueous liquid phase. The activities of individual species are further used in the electrochemical model. After completing speciation calculations, diffusion coefficients of individual species and viscosity of the solution are computed using separate models[23,24]. The electrochemical model[20,21] takes into account reactions on the surface of the metal and transport processes for the species that participate in the reactions. The model includes passivation phenomena, which may be influenced by pH and the presence of aggressive or inhibitive species in the solution. Further, the model combines the partial processes to compute corrosion rates in the framework of the mixed potential theory.

Anodic and Cathodic Reactions in the Active Range. The model includes expressions for partial anodic and cathodic processes, which may occur under activation or mass transport control. The expressions are in agreement with the generally accepted views on the mechanisms of partial processes. For example, the current density of iron dissolution is given by

$$i_{Fe} = i_{Fe}^0 \exp\left[\frac{\mathbf{a}_{Fe} F\left(E - E_{Fe}^0\right)}{RT}\right] \tag{3}$$

where the exchange current density is related to the activity of hydroxide ions and water molecules by

$$i_{Fe}^0 = i_{Fe}^* \frac{a_{OH^-}}{1 + K_{OH^-} a_{OH^-}} a_{H_2O}^c \tag{4}$$

where the symbol a denotes activity and K is a parameter. The rationale for eq. (4) was discussed in detail in a previous paper[21].

A typical example of a cathodic process is provided by the reduction of protons. It is generally accepted that the H^+ reduction reaction may proceed under activation or mass transfer control. Therefore, the current density for H^+ reduction can be written as

$$\frac{1}{i_{H^+}} = \frac{1}{i_{H^+,a}} + \frac{1}{i_{H^+,lim}} \tag{5}$$

where $i_{H^+,a}$ and $i_{H^+,lim}$ are the activation and limiting current densities, respectively. The activation current density for proton reduction is

$$i_{H^+,a} = i_{H^+}^0 \exp\left[\frac{-\mathbf{a}_H F\left(E - E_H^0\right)}{RT}\right] \tag{6}$$

with

$$i_{H^+}^0 = i_{H^+}^* a_{H^+}^{0.5} a_{H_2O}^{1.4} \tag{7}$$

The limiting current density in eq. (5) results from diffusion-limited transport of protons to the metal surface and can be calculated as

$$i_{H^+, \lim} = k_m F a_{H^+} \qquad (8)$$

where k_m is the mass transfer coefficient. The value of k_m can be calculated if the flow regime, diffusion coefficient of H^+ ions and solution viscosity are known. In near-neutral environments, water reduction is much more significant than proton reduction and therefore, a limiting current density is not observed[17].

Other important examples of partial electrode processes include:

- Reduction of water molecules
- Reduction of dissolved oxygen
- Reduction of carbonic acid, which is formed from dissolved carbon dioxide in a kinetically controlled reaction
- Reduction of oxidizing species such as chromates, nitrites, etc.
- Reduction of metal cations such as ferric or cupric ions

A more detailed discussion of these processes can be found in previous papers[20-22].

Adsorption effects.   The kinetics of the partial anodic and cathodic reactions is influenced by the adsorption of solution species (e.g., halide ions) on the surface. Adsorption may lead to a reduction in the effective surface area that is available to the partial processes. Adsorption coverage can be conveniently calculated using model such as the Frumkin isotherm:

$$K_i a_i = \frac{q_i}{1 - \sum_j q_j} \exp\left(\sum_j A_{ij} q_j \right) \qquad (9)$$

where θ_j is a fractional surface coverage and K_i and A_{ij} are constants. At some conditions, adsorption in halide solutions may lead to a change in dissolution mechanism and halide-accelerated dissolution. Accordingly, an additional contribution to the anodic current density arises due to the dissolution of metal-halide complexes[21] :

$$i_{Fe, X_k} = i^*_{Fe, X_k} a^s_{X_k^-} a^t_{OH^-} \exp\left(\frac{F(E - E^0_{Fe})}{RT} \right) \qquad (10)$$

Additional contributions to the anodic dissolution of iron may also be related to the adsorption of other components, such as sulfide species.

Active-passive transition.   The active-passive transition is introduced into the electrochemical model by considering a current that leads to the formation of a passive layer in addition to the current that leads to active dissolution. At any instant, a certain fraction of the surface q_P is assumed to be covered by a passive layer. The change of the passive layer coverage fraction with time can be expressed as

$$\left(\frac{\partial q_P}{\partial t} \right)_{E, a_i} = c i_2 (1 - q_P) - K q_P \qquad (11)$$

where i_2 is the current density that contributes to the formation of a passive layer. The second term on the right-hand side of eq. (11) represents the rate of dissolution of the passive layer, which is proportional to the coverage fraction. Solution of this equation in the steady-state limit yields an expression for the anodic dissolution current:

$$i_{Fe,TOT} = \frac{i'_{Fe} + i_2}{1 + \dfrac{ci_2}{K}} = \frac{i'_{Fe} + i_2}{1 + \dfrac{i_2}{i_P}} \tag{12}$$

where the ratio c/K constitutes the passive current density. This formulation can represent the observable characteristics of the active-passive transition.

Effect of Solution Chemistry on Passivity. In the absence of active ions, the passive current density depends primarily on the pH of the solution. Halide and other active ions cause the breakdown of passive films, which manifests itself in an increase in the passive current in addition to the onset of localized corrosion. On the other hand, corrosion inhibitors such as molybdates or chromates may repair passive films, thus reducing the passive current density. The effect of active species on the dissolution in the passive state can be modeled by considering surface reactions between the metal oxide film and solution species, i.e.,

$$\equiv\!FeO_aOH_b + c_iX_i \;=\; \equiv\!FeO_{di}(OH)_{fi}X_{ci} + e_iOH^- \tag{13}$$
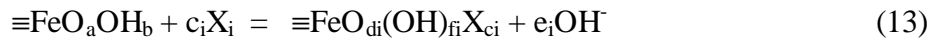
where the symbol $\equiv$ denotes a surface species and X_i is the i-th active species. In eq. (13), the stoichiometry is usually difficult to define because of the dynamic nature of the system and may be, in general, fractional. It is reasonable to assume that eq. (31) is in quasi-equilibrium and characterize it by an equilibrium constant. The surface species that forms as a result of reaction (13) may undergo irreversible dissolution reactions, i.e.,

$$\equiv\!FeO_{di}(OH)_{fi}X_{ci} + sH^+ \rightarrow Fe(OH)_g^{f+} + c_iX_i \tag{14}$$

and

$$\equiv\!FeO_{di}(OH)_{fi}X_{ci} + uH_2O \rightarrow Fe(OH)_3^{0} + c_iX_i \tag{15}$$
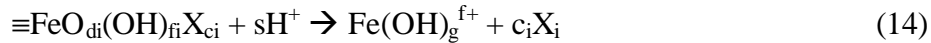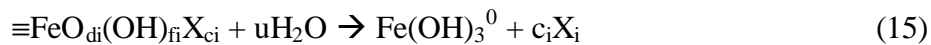
On the right-hand side of eqs. (14) or (15), the active anions may further form aqueous complexes with the hydrolyzed iron cations. Mathematical analysis[21] of reactions (13-15) yields a relationship between the passive current density and activities of reactive species, i.e.,

$$i_p = \left(k_H a_{H^+}^s + k_{H_2O} a_{H_2O}^u\right)\frac{1 + \displaystyle\sum_i l_i \frac{a_{X_i}^{c_i}}{a_{OH^-}^{e_i}}}{1 + \displaystyle\sum_i K_i \frac{a_{X_i}^{c_i}}{a_{OH^-}^{e_i}}} \tag{16}$$

Implementation of the model. The parameters of the electrochemical model are determined by utilizing a large number of experimental polarization and corrosion rate data. The partial electrochemical

processes described above are combined into a total predicted polarization curve. The corrosion potential is calculated by applying the mixed-potential theory, i.e.,

$$\sum i_{c,i} = \sum i_{a,j} \tag{17}$$

where $i_{c,i}$ and $i_{a,j}$ denote the i-th cathodic and j-th anodic process. Once the corrosion potential is obtained by solving eq. (17), the corrosion current density is also computed.

Sample results. In this study, the model has been applied to carbon and stainless steels in acids in order to illustrate the capabilities of the model for relatively simple aqueous environments. Figure 1 shows the calculated corrosion rates of carbon steel in sulfuric, phosphoric and hydrochloric acids. In this case, the corrosion is entirely in the active state. Thus, the observed corrosion rates result from the interplay between two predominant electrode processes, i.e., the anodic dissolution of iron and the cathodic reduction of protons. The observed differences in the corrosion rates in the three acids can be easily rationalized in terms of the model. The difference between sulfuric and phosphoric acid is simply due to differences in speciation, i.e., the lower activity of protons in phosphoric acid makes it less corrosive than sulfuric acid. In the case of hydrochloric acid, the corrosion rates are lower than those for H_2SO_4 for low and moderate concentrations of the acids. This is due to the adsorption of Cl ions on iron. At high HCl concentrations, the rate becomes higher because of halide-accelerated dissolution. Both effects are taken into account by the model.

It should be noted that the data shown in Figure 1 were used to regress the electrochemical parameters (i.e., the exchange current densities). The results shown in this figure can be regarded as a *correlation* of experimental data rather than a *prediction*. Therefore, it is worthwhile to verify the model by comparing *predicted* corrosion rates with experimental data that were not used to regress the model parameters. Such a comparison is shown in Figure 2 for carbon steel in acetic acid. In this case, the corrosion rate is determined by the speciation (which determines the activity of protons) and the kinetic processes of iron oxidation and proton reduction. Both kinetic processes are influenced by water activity as discussed by Anderko and Young[21]. The water activity effects manifest themselves in the decrease in the corrosion rate at high acetic acid concentrations, at which the water activity is reduced. The reaction orders with respect to water, which quantify the water activity effects were obtained from data on general corrosion in concentrated brines[21]. Thus, the corrosion rates shown in Figure 2 could be predicted without using the acetic acid data to fit corrosion rates.

The model is also applicable to stainless steels, in which active-passive transitions play a more significant role. Figure 3 shows the calculated corrosion rates of type 316 stainless steel in sulfuric and hydrochloric acids. Here, the trend is different from that observed for carbon steel (cf. Fig. 1) because HCl is more corrosive than H_2SO_4 at the same low and moderate molalities. This is due to the effect of chloride ions on the dissolution of oxide films. It is particularly interesting to examine the predictions of the model for the corrosion rates in mixed acid systems. An example of such calculations is shown in Figure 4 for the mixture of sulfuric and hydrochloric acids at 40 °C. When small concentrations of HCl are added to a 20% H_2SO_4 solution, the corrosion rate increases. This cannot be attributed to small changes in acidity. Rather, it is due to the effect of chloride ions on the active-passive transition. This effect is reproduced by the model and a reasonable agreement with the data of Sridhar et al.[25] is obtained.

Since the model is based on a combined electrochemical and thermodynamic view of general corrosion, it can predict the corrosion potential in addition to the corrosion rate. This is illustrated in Figure 5 for type 304 stainless steel in aerated acidic solutions. Here, a distinct jump in the corrosion

potential is observed as the pH is increased beyond a certain level. This jump is due to a transition from corrosion in the active state at strongly acidic conditions to corrosion in the passive state.

Localized Corrosion Prediction

Localized corrosion processes are of concern because the rate of growth of the corrosion front can be extremely high locally and localized corrosion can be a pre-cursor to other failure modes, such as stress corrosion cracking. Pitting and crevice corrosion are the two most often encountered forms of localized corrosion, although in specific alloy systems other localized corrosion modes, such as filiform corrosion, can be encountered. Localized corrosion processes are essentially stochastic in nature and therefore require a probabilistic approach to prediction.

It has been well established that localized corrosion is initiated when the corrosion potential exceeds a critical potential[26]. However, the applicability of the critical potentials measured using short-term electrochemical tests and the mechanistic bases for these potentials have been debated in the past[27]. Alternative methods to predict the occurrence of localized corrosion include, critical temperature and depassivation pH. While both the critical temperature and pH are useful for a ranking of alloy systems, the former having a greater sensitivity to alloy composition, they are not particularly useful to predict the occurrence of localized corrosion in a given process stream. In some applications (e.g., seawater), considerable experience has been gained on the use of various alloys and therefore a correlation between critical temperature and performance has been established. However, this is not the case for many chemical process streams.

The applicability of repassivation (or protection) potential to predict the occurrence of localized corrosion (stable pitting and crevice corrosion) has been demonstrated for many alloys[27]. The mechanistic bases for the repassivation potential and the relationship between pitting and crevice corrosion are still under debate[28,29]. While this may prevent the development of a first-principles model at this time, a semi-empirical model based on experimentally measured repassivation potentials can be constructed to predict the occurrence of localized corrosion. The corrosion potential can be calculated using the methodology described previously for general corrosion. The effect of applied and open-circuit potentials on the occurrence of localized corrosion on alloy 825 is shown in Figure 6[27]. The band of repassivation potential (E_{rp}) represent the range of measured values using various techniques including cyclic potentiodynamic polarization and stepwise decrease in potentials[27]. The open-circuit potentials were established through the use of various redox agents, such as Cu^+/Cu^{2+}. Both pitting and crevice corrosion samples are represented in this figure. At high applied or redox potentials, the initiation of pitting or crevice corrosion is extremely rapid, under applied or open-circuit potential conditions. As the potential approaches the repassivation potential, the initiation time increases markedly. At or below the repassivation potential, localized corrosion initiation has not been observed in over 4 years of exposure.

The dependence of repassivation potential on temperature and chloride concentration is shown in Figure 7 for alloy 22 (Ni-21.5 wt.%Cr-13 wt.%Mo-3 wt.%W-3 wt.%Fe). Independently of these tests, the critical crevice temperature of this alloy in $FeCl_3$ has been measured by others[30-31]. The corrosion potential and the calculated chloride concentration in $FeCl_3$ are also plotted on the same figure. The chloride concentration in $FeCl_3$ was calculated by the equilibrium speciation software described earlier. For concentrations of $FeCl_3$ below 1 molar (16.22 weight percent $FeCl_3$), the dissociation to chloride ion is essentially complete. A small concentration of chloride complexes ($FeCl_2^+$ and $FeCl^{2+}$) and solid $Fe(OH)_3$ are predicted and observed experimentally[31]. Therefore 6 weight percent $FeCl_3$, used commonly in standard tests[30], corresponds to about 1.1 M of Cl^-. The critical crevice temperature of alloy 22 in 6 to 10 weight percent $FeCl_3$ has been reported to range from 55°C to over 80°C. As shown

in Figure 7, the corrosion potential of alloy 22 in this solution exceeds the repassivation potential at 80°C and therefore occurrence of localized corrosion would be expected. The repassivation potential at about 50-55°C has not been reported, but is expected to be high based on measurements of less alloyed materials. These results suggest that the short-term electrochemical measurements of repassivation potentials and corrosion potential in NaCl solutions can be used to predict the performance of the same alloy in other chloride environments containing redox species. The repassivation potentials of three different Ni-base alloys are shown in Figure 8. Because the solubility of NaCl is around 5.5 molar, LiCl solutions were used for higher concentrations of chloride. The repassivation potential is not dependent on the pH because the localized corrosion sites are highly acidic regardless of the pH of the bulk solution[26,27]. A comparison of the anticipated localized corrosion resistance of a number of candidate alloys can be made in other chloride containing environments using this type of data generated in NaCl and LiCl solutions. A computer code for probabilistic prediction of pitting failure using this methodology has been discussed elsewhere[32]. In more complex environments such as, HNO_3+HCl mixtures, the behavior of alloys would depend on the NO_3/Cl^- ratio and alloy composition[25].

The growth rate of localized corrosion is governed by a combination of cathodic reduction processes, ohmic potential drop in the growing pits, and the transport of metal cation complexes away from the growing pit front[26,27,33]. An example of crevice corrosion growth is shown for type 316L stainless steel in chloride solution in Figure 9. Although the data indicates crevice corrosion growth, the growth of crevice corrosion occurred in the form of pits within the crevice regions perpendicular to the crevice face. The data indicates that in one year, the crevice corrosion will propagate through 1.5 cm. In this example, as in many complex situations encountered in the process industries, the rate controlling process is not always known. However, bounding calculations may be performed to conservatively estimate the failure time. Such a bounding rate may be determined by the outward transport of metal ion complexes. The initiation time combined with growth rate of localized corrosion can then be used to predict the failure time for a given component. It should be noted that the failure time may not always be the time for complete penetration of the wall of a vessel or piping. Depending on the mechanical loading (internal pressure etc.), a defect size less than the wall thickness may lead to mechanical failure[32].

EMPIRICAL AND HEURISTIC MODELS

Empirical Models

This type of models is suitable when the chemistry of the aqueous stream is limited in scope and plentiful experimental data are available for determining the model parameters. For example, correlations have been successfully used to model CO_2 corrosion of carbon steel[34-37]. For localized corrosion of stainless steels and Ni-base alloys, a number of correlations in the form of Pitting Resistance Number (PRN) have been developed. The PRN approach is only useful for the relative ranking of alloys in a specific type of environment and does not enable prediction of the alloy performance, except in cases where prior service experience has been gained. Alternatively, for a given set of environmental compositions, multiple regression analysis of the pitting resistance versus the various anionic concentrations can be made[38]. The main limitation of this approach is its lack of validity outside the range of environmental and alloy variables included in the experiments. Approaches to developing empirical correlations have also been established for flow-induced corrosion in various systems[39].

Expert systems

Expert systems are conceptually similar to semi-empirical correlations and may include several individual correlations that cover various physical aspects of the process in addition to electrochemical

corrosion (e.g., multiphase flow effects). They also may include facilities for recommending materials for service in the presence of target environments. For example, the Materials Technology Institute (MTI) has developed a series of expert system advisors to select process equipment materials for service in the most common hazardous chemicals (the CHEM*COR modules). These models address selected single-component process environments. Several expert systems have been developed for CO_2 corrosion of carbon steels[40-43]. An expert system for localized corrosion in marine environments has been discussed by Hakkarainen[44]. This method uses the empirical dependence of critical temperature on chloride concentration, alloy composition, and flow rate. While the expert systems are valuable because they incorporate the plant experience in realistic systems, they are limited by the inability to reliably extrapolate beyond the experience base.

SUMMARY

Computer simulation of corrosion processes and incorporation of these tools in process design tools will be important in future operations of the chemical process industries. Mechanistic, semi-empirical, empirical, and expert system approaches were reviewed in this paper. A mechanistic approach to modeling general corrosion rates coupled with thermodynamic speciation calculations was described and examples were given. Such an approach is useful because it has the potential for being readily incorporated in existing process simulation tools. An approach to extending this model to predicting localized corrosion, based on repassivation and corrosion potentials, was outlined. For predicting localized corrosion, a semi-empirical approach is necessary because of the complexity of the lack of agreement on the governing mechanisms. Examples of localized corrosion were cited and the measurements made in simple NaCl and LiCl solutions were extrapolated to observations in more complex chloride solutions.

ACKNOWLEDGMENT

REFERENCES

1. G.E. Keller, II and P.F. Bryan, Chemical Engineering Progress, p. 41, January 2000.

2. Materials Technology Institute of the Chemical Process Industries, Inc., "Technology Roadmap for Materials of Construction, Operation and Maintenance in the Chemical Process Industries", St. Louis, MO, December 1998.

3. T. Edgar, Chemical Engineering Progress, p. 51, January 2000.

4. R.W. Staehle, "Combining Design and Corrosion for Predicting Life," in Life Prediction of Corrodible Structures, R.N. Parkins, ed. (Houston, TX: NACE International), p. 138-291.

5. K. S. Pitzer (ed.), Activity Coefficients in Electrolyte Solutions, 2nd ed., CRC Press, Boca Raton, FL (1991).

6. J. R. Loehe and M. D. Donohue, AIChE J., 43, p. 180 (1997).

7. J.F. Zemaitis, Jr., D. M. Clark, M. Rafal, N. C. Scrivner, Handbook of aqueous electrolyte thermodynamics: AIChE, New York, NY, 852 p. (1986).

8. M. Rafal, J. W. Berthold, N. C. Scrivner, S. L. Grise, Models for electrolyte solutions, *in* S. I. Sandler, ed., Models for Thermodynamic and Phase Equilibria Calculations: M. Dekker, New York, NY, p. 601-670 (1995).

9. H. C. Helgeson, D. H. Kirkham, G. C. Flowers, Am. J. Sci., v. 281, p. 1249-1516 (1981).

10. J. C. Tanger, H. C. Helgeson, Am. J. Sci., v. 288, p. 19-98 (1988).

11. E. L. Shock, H. C. Helgeson, Geochim. Cosmochim. Acta, v. 52, p. 2009-2036 (1988).

12. E. L. Shock, H. C. Helgeson, Geochim. Cosmochim. Acta, v. 54, p. 915-943 (1990).

13. D. A. Sverjensky, Reviews in Mineralogy, v. 17, p. 177-209 (1987).

14. L. A. Bromley, AIChE J., v. 19, p. 313-320 (1973).

15. K. S. Pitzer, J. Phys. Chem., v. 77, p. 268-277 (1973).

16. H. P. Meissner, *in* S.A. Newman, ed., Thermodynamics of Aqueous Systems with Industrial Applications: Am. Chem. Soc. Symp. Ser., v. 133, p. 495-511 (1980).

17. S. Nesic, J. Postlethwaite, S. Olsen, Corrosion, v. 52, p. 280-294 (1996).

18. E. Dayalan, F. D. de Moraes, J. R. Shadley, S. A. Shirazi, E. F. Rybicki, CORROSION/98, paper no. 51, NACE International, Houston, TX (1998).

19. D. D. Macdonald, M. Urquidi-Macdonald, Corrosion, v. 46, p. 380-390 (1990).

20. A. Anderko, R.D. Young, CORROSION/99, paper no. 31, NACE International, Houston, TX (1999).

21. A. Anderko and R. D. Young, Corrosion, 56, p. 543-555 (2000)

22. A. Anderko, P. McKenzie and R. D. Young, CORROSION/2000, paper no. 479, NACE International, Houston, TX and Corrosion, in press (2000)

23. A. Anderko, M. M. Lencka, Ind. Eng. Chem. Res., v. 37, p. 2878-2888 (1998).

24. M. M. Lencka, A. Anderko, S.J. Sanders, R. D. Young, Int. J. Thermophysics, v. 19, p. 367-378 (1998).

25. N. Sridhar, J. B. C. Wu, S. M. Corey, Materials Performance, v. 26, p. 17, October (1987).

26. Z. Szkalarska-Smialowska, Pitting Corrosion of Metals, NACE International, Houston, TX (1986).

27. D.S. Dunn, G.A. Cragnolino, and N. Sridhar, Corrosion, v. 56, p. 90 (2000).

28. N.J. Laycock and R.C. Newman, Corrosion Science, v. 39, p. 1771 (1997)

29. N.J. Laycock, J. Stewart, and R.C. Newman, Corrosion Science, v. 39, p. 1791 (1997).

30. E.L. Hibner, Materials Performance, v.26, p. 37 (1987).

31. M. Renner, U. Heubner, M.B. Rockel, and E. Wallis, Werkstoffe u. Korrosion, v. 37, p. 183 (1986).

32. G.A. Cragnolino, S. Mohanty, D.S. Dunn, N. Sridhar, and T.M. Ahn, Nuclear Eng. Design, (2000).

33. H.S. Isaacs, J. of Electrochem. Soc., v. 120, p. 1456 (1973).

34. B.de Waard, D. E. Milliams, Corrosion, v. 31, p. 177-181 (1975).

35. B.de Waard, U. Lotz, D. E. Milliams, Corrosion, v. 47, p. 976 (1991).

36. L. K. Gatzky, R. H. Hausler, "A Novel Correlation of Tubing Corrosion Rates and Gas Production Rates", *in* R.H. Hausler, H. P. Goddard, Advances in CO_2 Corrosion, Vol. 1, p. 87, NACE

International, Houston, TX (1984).

37. R. C. John, K. G. Jordan, A. L. Young, S. D. Kapusta, W. T. Thompson, CORROSION/98, paper no. 20, NACE International, Houston, TX (1998).

38. G.A. Cragnolino and N. Sridhar, Corrosion, v.47, p. 464 (1991).

39. NACE Publication 5A195, State-of-the-Art Report on Controlled-Flow Laboratory Corrosion Tests, NACE International, Houston, TX (1995).

40. S. Srinivasan, R. D. Kane, CORROSION/96, paper no. 11, NACE International, Houston, TX (1996).

41. J. D. Garber, F. H. Walters, R. R. Alapati, C. D. Adams, CORROSION/94, paper no. 25, NACE International, Houston, TX (1994).

42. M. R. Bonis, J.-L. Crolet, CORROSION/89, paper no. 466, NACE International, Houston, TX (1989).

43. R. Zhang, M. Gopal, W. P. Jepson, CORROSION/97, paper no. 601, NACE International, Houston, TX (1997).

44. P. B. Mathur, T. Vasudevan, Corrosion, v. 38, p. 171 (1982).

45. M.M. Singh, A. Gupta, Corrosion, 56, p. 371 (2000).

46. L. L. Shreir (ed.), Corrosion, Metal/Environment Reactions, vol. 1, Newness-Butterworth, Boston (1976).

47. H.P. Leckie, Corrosion, 24, p. 70, (1968)
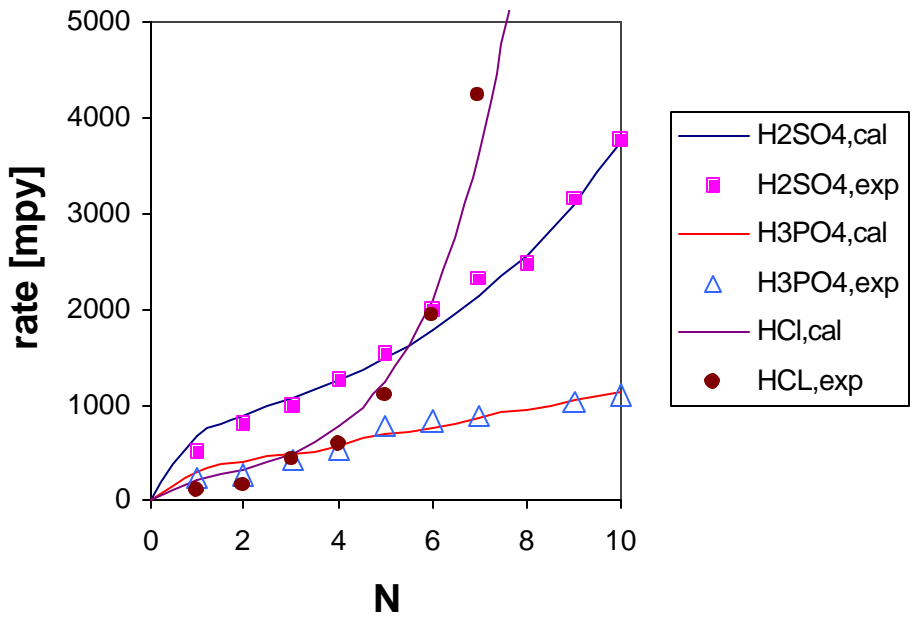
Figure 1. Corrosion rates of carbon steel in sulfuric, hydrochloric and phosphoric acids at 33 °C. The symbols denote the data of Mathur and Vasudevan[44]. The lines have been obtained from the corrosion rate model by regressing electrochemical parameters to match experimental data.
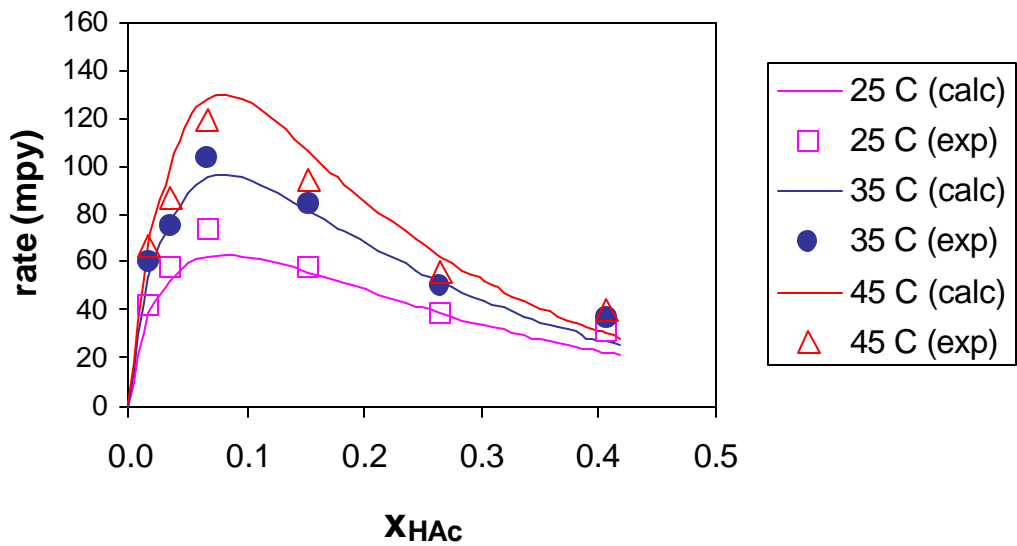
Figure 2. Corrosion rates of carbon steel in aqueous acetic acid. The symbols denote the data of Singh and Gupta[45]. The lines have been obtained from the model without using the acetic acid data to regress electrochemical parameters.
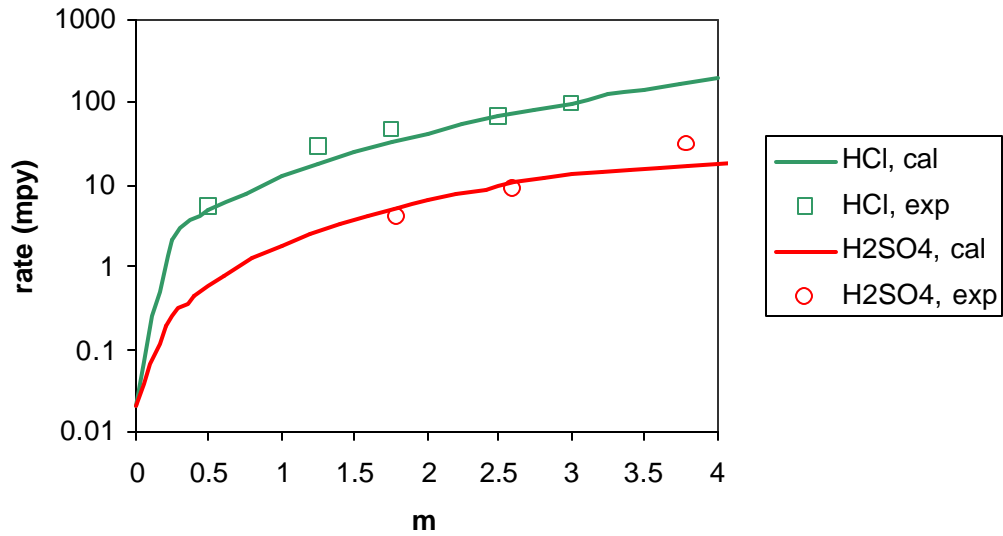
Figure 3. Corrosion rates for type 316 stainless steel in sulfuric and hydrochloric acids. The symbols denote experimental data[46] and the lines have been obtained from the model.
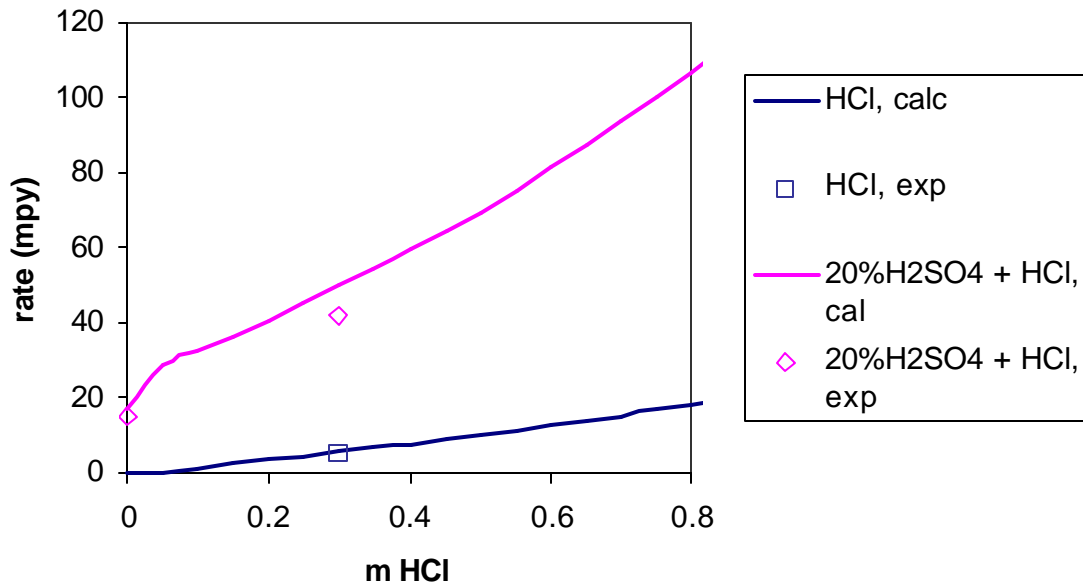
Figure 4. Effect of HCl concentration on the corrosion rate of type 316 stainless steel. The lower line shows the corrosion rate in pure HCl solution and the upper line shows the rate in a 20% H_2SO_4 solution with varying concentrations of HCl added to the system. The symbols denote the data of Sridhar et al.[25].
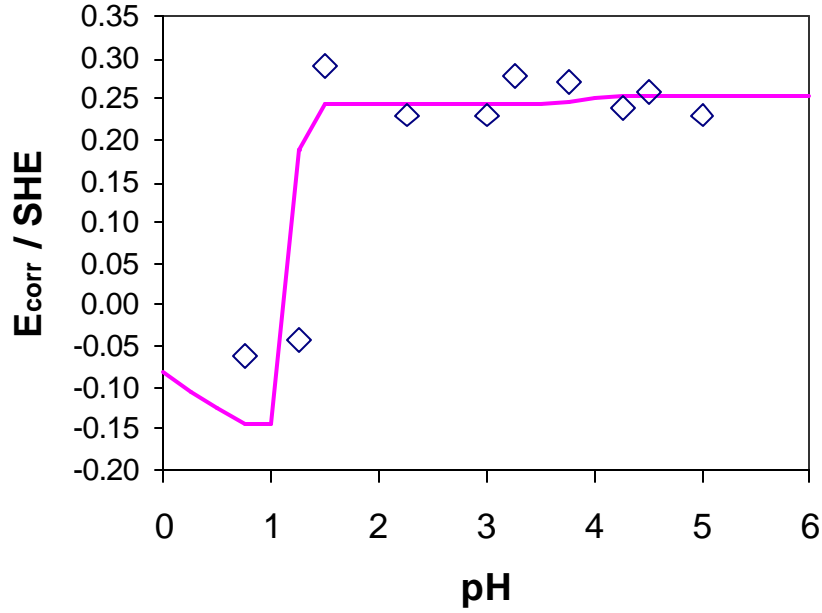
Figure 5. Corrosion potential for type 304 stainless steel as a function of pH in an aerated sulfuric acid solutions. The symbols denote the data of Leckie[47] and the line has been obtained from the model.
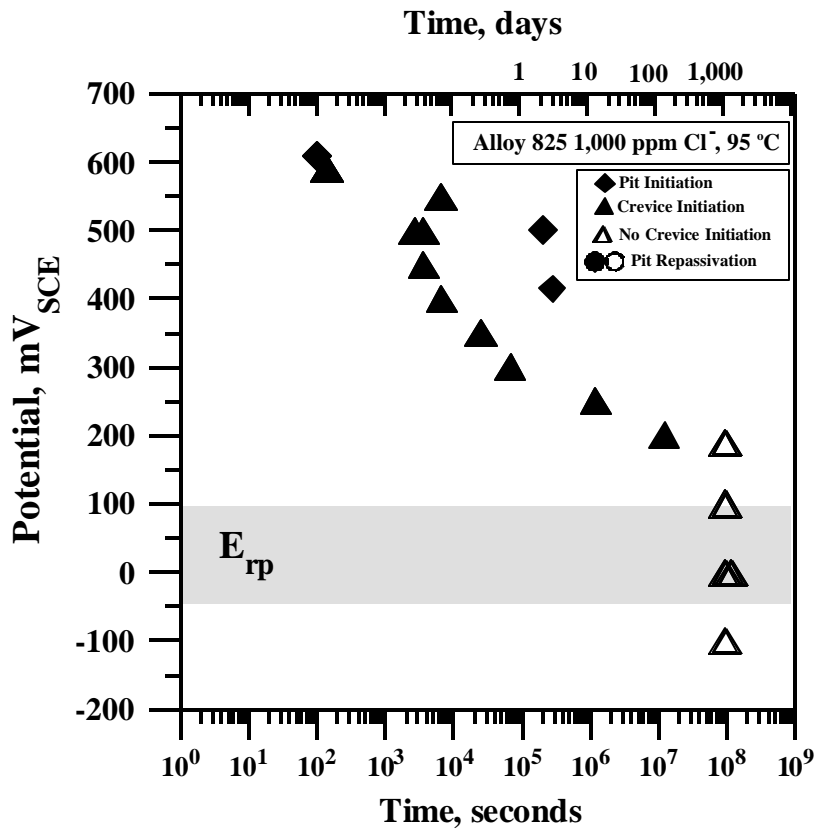
Figure 6. Effect of potential on time to initiate pitting and crevice corrosion of a Ni-base alloy, alloy 825 in a chloride containing groundwater[27].
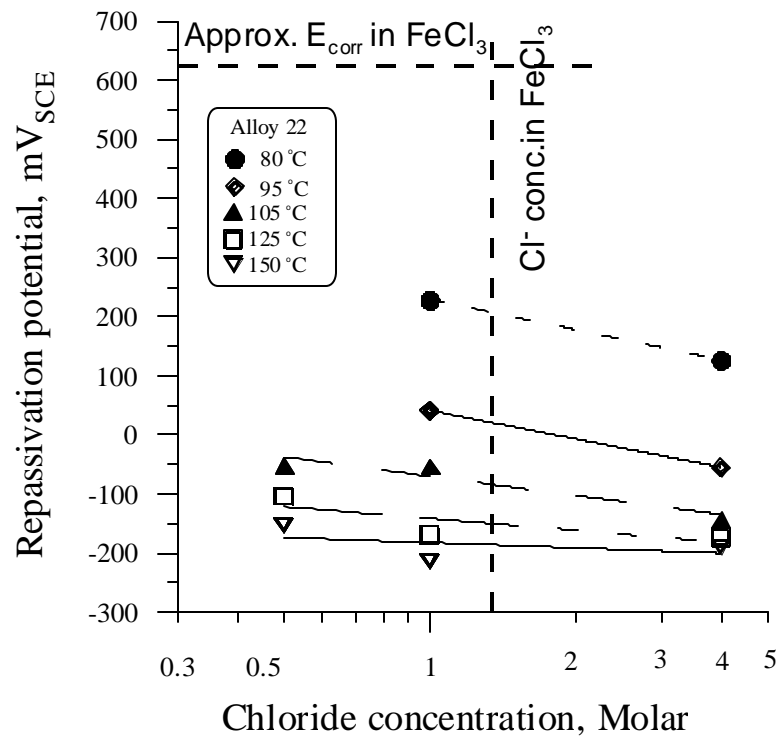
Figure 7. Effect of temperature and chloride concentration on repassivation potential of alloy 22 in NaCl solutions. The chloride concentration and corrosion potential in 6 wt. Percent FeCl₃ are superposed to indicate the crevice corrosion susceptibility of alloy 22 in FeCl₃ above 80° C.
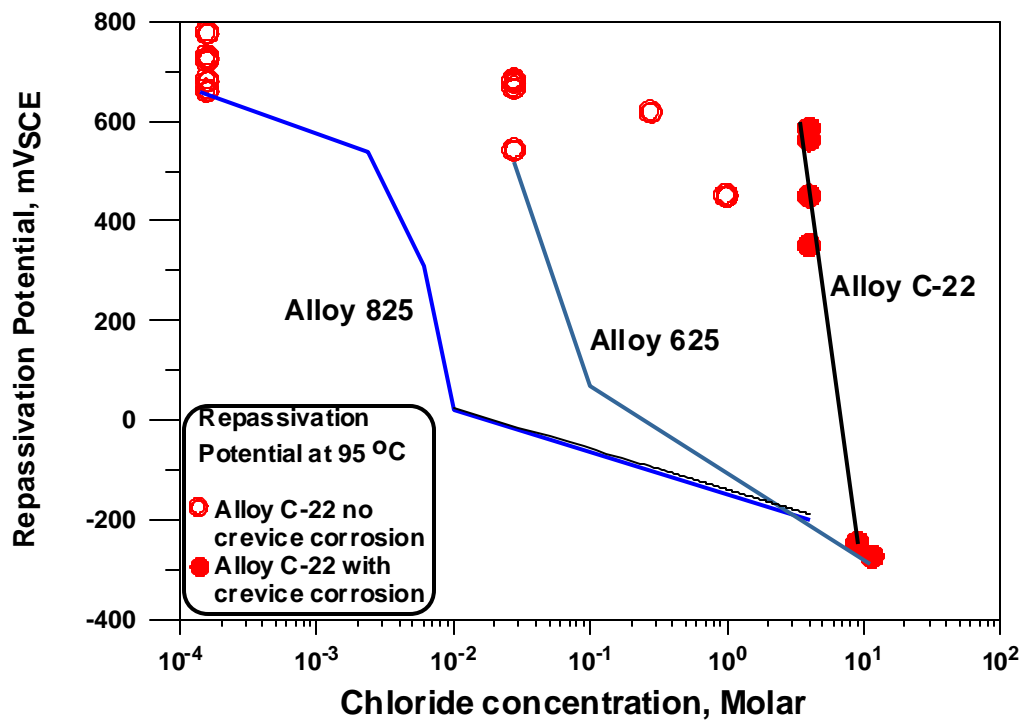
Figure 8. Effect of chloride concentration on the repassivation potential of three Ni-base alloys in NaCl and LiCl solutions.
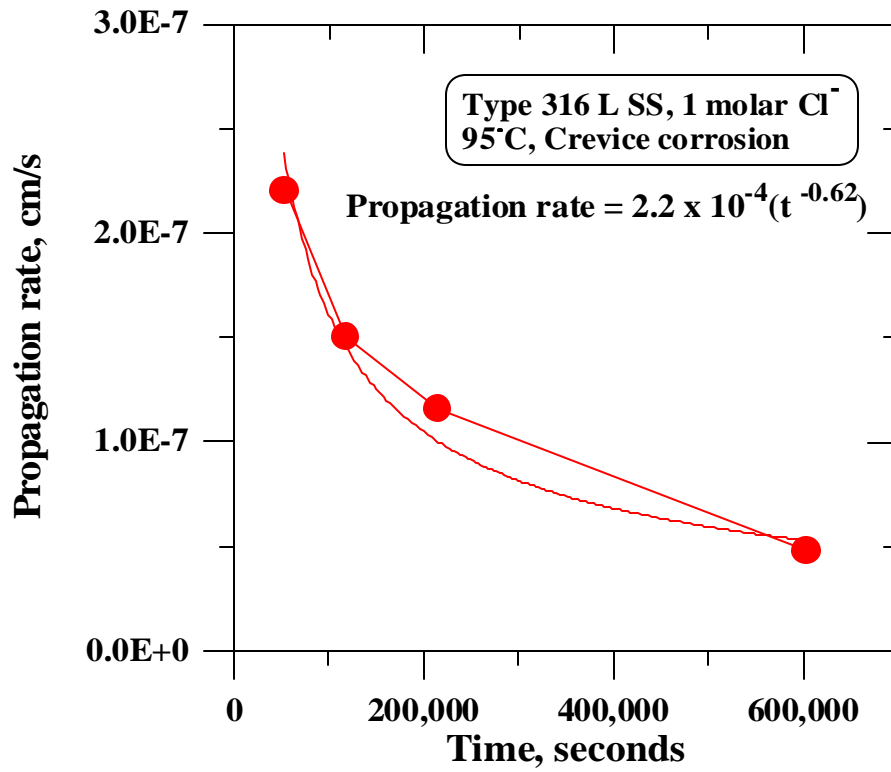
Figure 9. The growth rate of crevice corrosion perpendicular to the crevice face on type 316L stainless steel in NaCl solution at 95°C under open-circuit conditions (aerated)[27].